



A REVIEW OF AERONAUTICAL FATIGUE AND STRUCTURAL INTEGRITY IN ISRAEL (2019 –2021)



Compiled by:
Dr. Yuval Freed
Engineering Division
Israel Aerospace Industries
Ben-Gurion Airport, Israel
yfreed@iai.co.il



A REVIEW OF AERONAUTICAL FATIGUE AND STRUCTURAL INTEGRITY IN ISRAEL

JANUARY 2019 – DECEMBER 2020

SUMMARY

This review summarizes fatigue, structural-integrity and fracture-mechanics investigations that were performed in Israel during the period of January 2019 to December 2020. The review includes contributions from Israel Aerospace Industries Ltd. (IAI), Tel-Aviv University (TAU), Technion Institute of Technology, Ben-Gurion University (BGU), Bird Aerosystems and Brot Engineering Consultant.



TABLE OF CONTENTS

1.	INTRODUCTION	4
2.	FATIGUE ANALYSIS, TESTING AND LIFE EXTENSION	5
3.	STRUCTURAL INTEGRITY OF COMPOSITE MATERIALS	21
4.	STRUCTURAL HEALTH MONITORING	27
5.	MISCELLANEOUS.....	32
7	REFERENCES	37



A REVIEW OF AERONAUTICAL FATIGUE INVESTIGATIONS IN ISRAEL JANUARY 2017 – DECEMBER 2018

1. INTRODUCTION

The Israel National Review summarizes activities performed in the field of aeronautical fatigue, structural integrity, health monitoring and fracture mechanics in Israel during the period of January 2019 to December 2020. The previous National Review [1] covered activities up to the end of 2018. The following organizations contributed to this review:

- Israel Aerospace Industries Ltd. (IAI)
- Tel-Aviv University (TAU)
- Technion Institute of Technology
- Ben-Gurion University (BGU)
- Bird Aerostructures
- Abraham Brot – Brot Engineering Consultant

The National Review was compiled by Dr. Yuval Freed (yfreed@iai.co.il).

2. FATIGUE ANALYSIS, TESTING AND LIFE EXTENSION

2.1 Widespread Fatigue Damage – What could possibly go wrong? (Y. Freed, IAI)

Widespread fatigue damage is probably the most urgent structural integrity concern the aviation industry deals with these days. Specifically, Widespread Fatigue Damage (WFD) phenomenon is a simultaneous evolution of cracks at multiple structural locations that are of sufficient size and density such that the crack can no longer meet its residual strength requirements. Widespread fatigue damage is accounted for as part of the design of new products, and should be substantiated by analysis supported by test evidence, preferably a full scale test evidence.

To this end, the author and his co-worker have published several papers in recent years introducing a new risk-assessment based approach for determination of inspection program to protect the structure from a WFD threat [3, 4]. This approach was implemented to investigate a very special case of the South Airlines accident in 2011. On April 1, 2011, a Boeing 737-300 airplane operated as Southwest Airlines (flight 812) experienced a rapid decompression during flight. The pilots conducted an emergency descent and diverted to Yuma International Airport in Arizona. Of the 5 crewmembers and 117 passengers on board, one crewmember and one nonrevenue off-duty airline employee passenger sustained minor injuries. The airplane sustained substantial damage; post-accident inspections revealed that a section of fuselage skin about 60 inches long by 8 inches wide had fractured and flapped open on the upper left side above the wing. At the time of the accident, the airplane has accumulated 39,786 flights, while its Limit of Validity (LOV) is 75,000 flights, and Boeing's Service Bulletin [5] calls for panel replacements at 50,000 flights (in WFD evaluation terminology this may be referred to as the lap joint SMP). Picture of the airplane on ground after landing is shown in Figure 1.



Figure 1: Photograph of Southwest Airlines flight 812 airplane on ground.

A comprehensive investigation was conducted to derive the root cause of this failure [6]. Microscopic examination of the longitudinal portion of the fracture surfaces revealed fracture features consistent with fatigue cracking that originated from 54 out of 58 rivet holes. The fatigue cracks emanated from the outer surface of the lower skin, which is not visible from the interior or exterior of the airplane. In nine adjoining rivet holes fatigue cracking occurred through 100% of the skin thickness. The two longest fatigue cracks were found on the forward and aft side of one of the holes (indicated as 'hole 85', see Figure 2), measured as 0.55 and 0.60 inches, respectively. The calculated total number of cycles for the longest fatigue crack at the critical rivet hole was 38,261 flight cycles, which was within about 1,500 cycles of the total cycles on the airplane. Illustrations of the crack pattern and the lap-joint structural detail are shown in Figure 2.

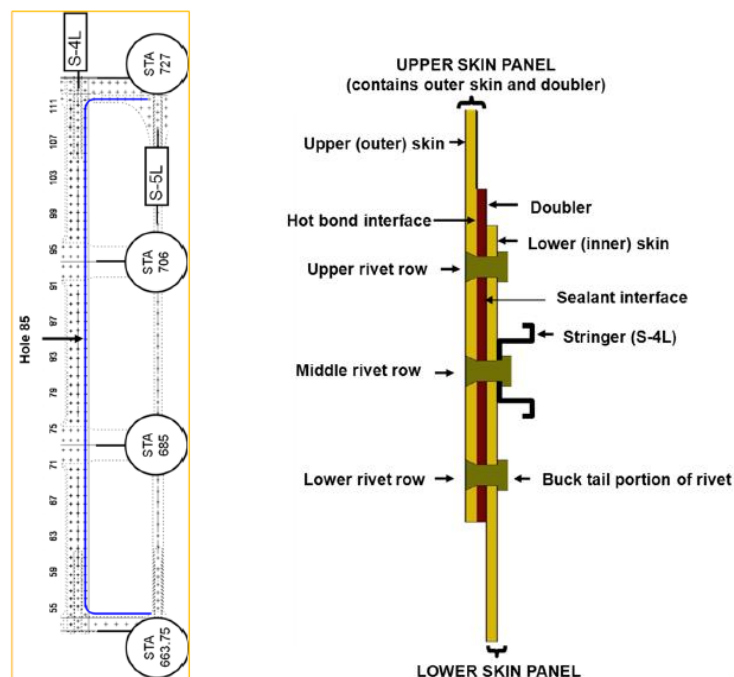


Figure 2: Typical skin longitudinal lap joint (left) and the crack pattern (right).

Examination of the rivets in the fracture area revealed numerous anomalies, including oversized rivets, variations in finish, under-driven conditions, expanded shank areas, and crank-shafting. Most of the lower-row holes in the lower skin had discrepancies including ovalized holes, double-drilled holes, gaps between the buck tail and the hole, sealant in the rivet hole, and burrs protruding from under the buck tail. Examination of the lap joint before it was separated revealed that almost all of the lower-row holes in the lower skin were offset from the holes in the upper skin and attached doubler. Based on the panel marking *it was concluded that the panel was replaced during assembly, and the evidences indicate that during drilling of the lap joint, the crown skin panel and the upper left fuselage panel were misaligned, so most of*



the lower rivet row holes were misdrilled. Many of the installed rivets did not completely fill the holes in the lower skin panel, which significantly reduced the fatigue life of the panel.

It may be noted that the damage tolerance philosophy assumes a 'rogue flaw' of large size, emanating at critical location in the airplane principal structural elements. Widespread fatigue evaluation on the other hand, deals with natural cracks that develop as the airplane approaches its design life goal. The case studied here is a special case that is not covered by these philosophies. On one hand, the cracks are definitely not natural (they are induced by improper installation of large panels), and therefore, they will reach a significant size prior to the ISP threshold inspection determined by WFD evaluation. On the other hand, there are multiple cracks that are nucleating from adjacent fasteners holes, and the corresponding residual strength of the panels is reduced significantly prior to standard damage tolerance based inspections.

This study [2] assessed the effect of such improper manufacture on the structural integrity of the airplane in line of the damage tolerance philosophy and the WFD evaluation. The risk analysis incorporated data from the fractographic examination of the cracked panel, in which the crack initiation period was only 1,500 flights, with crack growth lifetime of 38,261 flights. The critical crack length was reported as 0.6 inches [6]. By accounting for the inspection capabilities of the concerned regions, the scheduled inspection program of this structural detail and its life limitation, the Cumulative Probability of Failure (CPOF) was obtained. Figure 3 presents an illustration of the CPOF for the concerned case with various threshold and repeated inspection periods. In this analysis, it is assumed that the SMP is 50,000 flights. Acceptable CPOF (~0.01% - 0.001%) is reached only if the threshold inspection is performed at ~15,000 flights, with recurring inspections every 6,000 flights. It may be noted that the OEM instructions for inspections are at 28,000 flights with subsequent inspections every 12,000 flights. These instructions are obviously not sufficient for the southwest accident specific case.

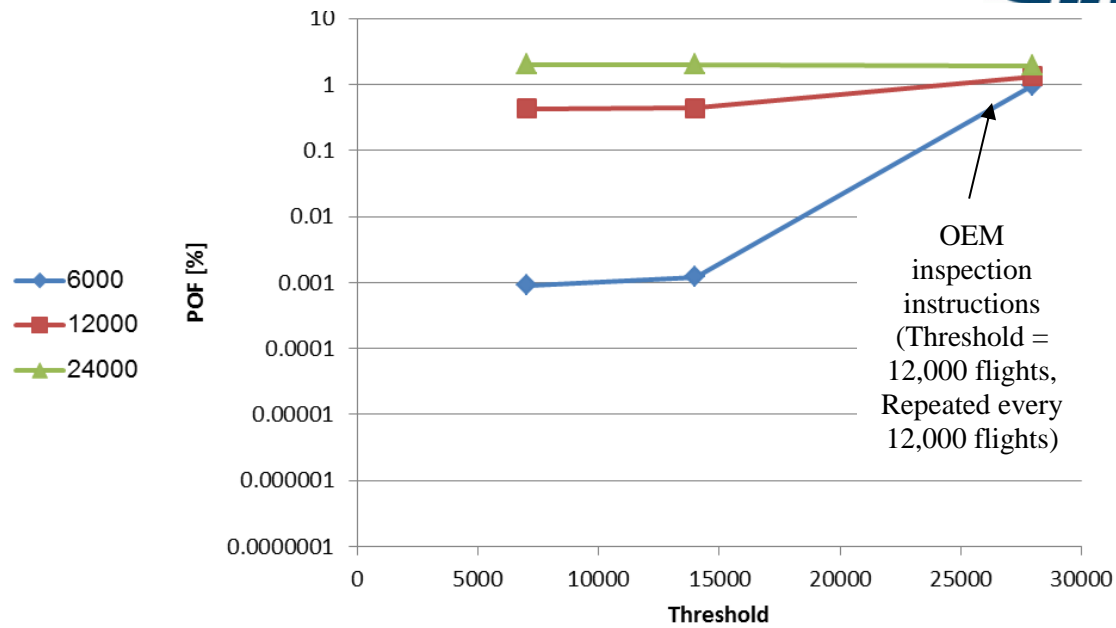


Figure 3: Cumulative Probability Of Failure (CPOF) for a "Southwest accident" lap joint analysis with crack initiation period of 1,500 flights, and crack growth lifetime of 38,261 flights. The effect of threshold inspection periods and repeated inspection intervals are shown.

At this point it is interesting to question ourselves whether additional rulemaking is required to address such rare cases. Boeing inspected hundreds of fuselage skins that were manufactured at the time of the concerned fuselage, and no similar findings of multiple site damage in the lap joints (as reported by Southwest Airlines) were reported. Thus, the NTSB concluded that it is unlikely that there was a systemic quality assurance error at the Boeing facilities at the time of manufacture. It is clear that additional restrictions, conservatism, and rulemaking will become a financial burden with some weight penalty. This will reflect on the aircraft performance, and will eventually increase flight costs. It is interesting to learn that the National Highway Traffic Safety Administration reported in 2008 on 1.27 fatalities per 100 million vehicle miles travelled. On the other hand, the National Transportation Safety Board reported on only 20 air accidents for U.S. air carriers in 2008. This works out to nearly zero accidents per million flying miles. No one died, and only five people were seriously injured. Increase flight costs can potentially lead to increase motor vehicle ground transportation, which is not as safe as air-traffic. Additional limitations, conservatism, and rule-making for such rare event are thus questionable.

The full length paper was presented in the 59th Israel Annual Conference on Aerospace Sciences in 2019 [2].

2.2 Investigation of the Effect of Secondary Bending on Multi-Site Damage Scenarios in Hard-point Joints (Y. Freed, IAI)

Typical fuselage structures consist of several structural details joined together by means of mechanical fasteners. Several of these structural concepts are shown in Figure 4 below. The fatigue performance of those elements, and especially the fatigue characteristics of their joints, can be a primary limitation to the endurance and safety of a traditional transport category airplane fuselage.

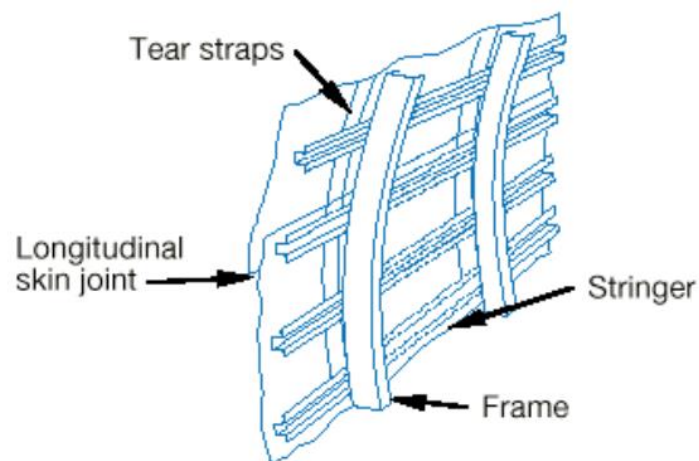


Figure 4: Typical fuselage structural details.

Hard-points are attachments in which the load is jointly carried by two or more members. Typical hard-points that may be found in fuselage structure are skin-doublers attachments and skin-stringers attachments. An example of an hardpoint is shown in Figure 5.

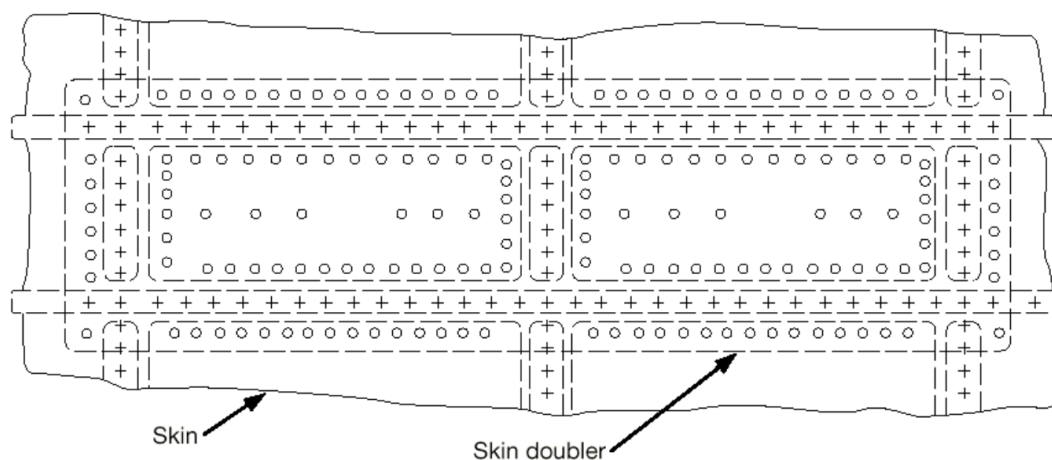


Figure 5: An example of skin-doubler attachment

Widespread Fatigue Damage (WFD) is the simultaneous presence of cracks at multiple structural locations that are of sufficient size and density such that the structure will no longer

meet its required residual strength. A good example of WFD is a Multiple Site Damage (MSD), in which the damage is characterized by the simultaneous presence of fatigue cracks in the same structural element. Illustration of MSD is provided in Figure 6.

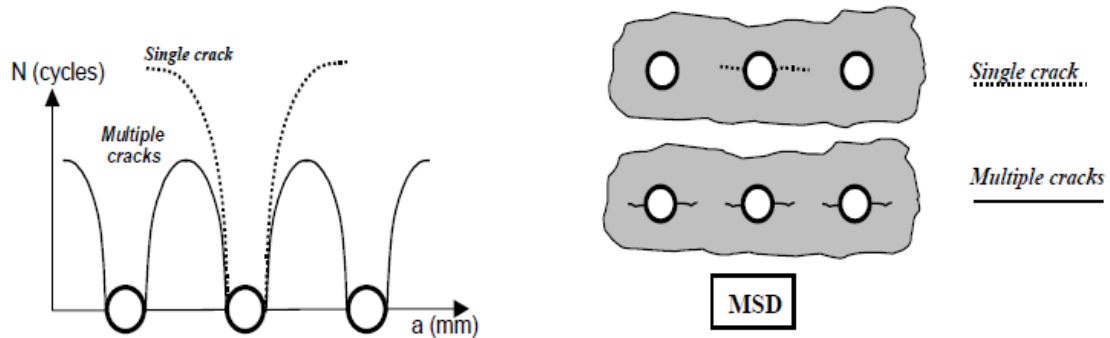


Figure 6: Multiple Site Damage (MSD) interaction effects

Hard-point attachments, as shown in Figure 5, are considered as candidates for MSD scenarios due to the fact that almost all the fasteners in each row of fasteners attaching the doubler to the skin are subjected to very similar loads (resulting in membrane stresses) upon cabin pressurization. Thus, it is reasonable to assume that natural crack will nucleate in adjacent fasteners in the hard-point. In addition, fastened attachments as hard-points include inherent eccentric with respect to the load path, which induces out of plane deflections of the skin sheets. This is referred to as secondary bending, and it is considered as a side effect of tensile membrane loads acting on the skin.

The secondary bending phenomenon was investigated mainly to lap-joint attachments [7-13]. As discussed in Ref. [88] for example, it can reach up to $k = 3$ for a case of a lap joint with a single row of rivets. This is a significantly increase of the stress level at the critical location of the joint. Analytical and numerical investigation of secondary bending in hard-point attachment were presented in recent publications [14, 15]. The conclusions drawn from analytical model presented in Ref. [15] showed that the expected increase in local stresses due to secondary bending in hard-point attachment of typical applications are up to 20%. This was validated by means of a numerical investigation [14, 15].

The current study focuses on the effect of the induced secondary bending on the inspection program defined to ensure that no failure occurs during service upon MSD. To this end, a typical case of skin reinforcement by a doubler is investigated, with several combinations of skin to doubler thicknesses. The induced secondary bending for each combination is obtained, as well as the expected reduction in WFD average lifetime and the corresponding ISP, SMP and inspection intervals. Figure 7 below provides an example of the effect of the secondary bending on the required inspection intervals. $ISP = 60,000$ flights, with $SMP = 75,000$ flights, and several inspection intervals were examined. It may be easily observed that the probability of failure increases significantly with the increase of the secondary bending effect to 20% of the

membrane stresses. However, the effect of 10% bending stresses is not that significant. Similar calculation was conducted for $ISP = 20,000$ flights and $40,000$ flights, and similar conclusions were drawn. In addition, the inspection intervals have minor effect due to the fact that the ISP was set as $60,000$ flights, with SMP taken as $75,000$ flights, and due to the relatively short critical crack length for a MSD scenario.

The full length paper was presented in the 60th Israel Annual Conference on Aerospace Sciences in 2020 [16].

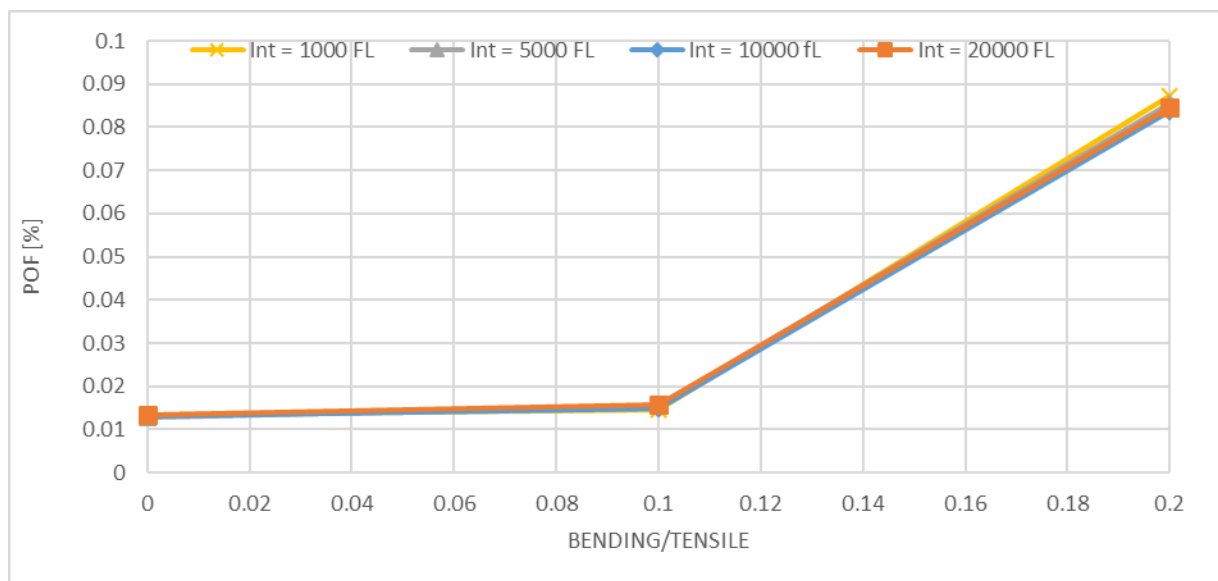


Figure 7: Effect of secondary bending on the probability of failure for a given scenario of $ISP = 60,000$ flights, $SMP = 75,000$ flights

2.3 Loss of Useful Consciousness Aboard an Aircraft due to a Lack of Oxygen (A. Brot, A. Brot Engineering Consultants)

Sudden decompression of the fuselage typically accompanies the loss of structural integrity of an aircraft fuselage. The Comet failures (1954) and the Aloha Airlines incident (1988) are two prime examples of sudden decompression resulting from a structural failure. In addition to the threat posed by the loss of structural integrity of the aircraft, there is another threat to consider. Sudden decompression could cause passengers and flight crew to lose consciousness, due to a lack of oxygen (hypoxia) at high altitudes. An example is the Southwest Airlines incident of 2011, where a flight attendant and a passenger lost consciousness during a sudden decompression. They recovered when the diving aircraft reached an altitude of about 10,000 feet [6].

The FAA issued advisory circular AC 61-107A in 2003 to address the topic of loss of useful consciousness, which was later modified in 2013 to AC 61-107B. It was then determined that the modified document did not address all of the NTSB's concerns about the time of useful



consciousness (TUC). In 2015, the FAA issued AC-61-107B CHG 1, which is currently in use. The times of useful consciousness detailed in this AC have been established from observations over a period of years, and are for an individual at rest. Any exercise will reduce the time considerably. For example, upon exposure to hypoxia at 25,000 feet, an average individual has a TUC of 3 to 5 minutes. The same individual, after performing 10 deep knee bends, will have a TUC in the range of only 1 to 1.5 minutes. Rapid loss of aircraft pressurization dramatically reduces TUC. As a general rule, it can be assumed that the TUC following rapid decompression at altitudes between 25,000 ft and 43,000 ft will be reduced by about 50 percent. Above 43,000 ft, the TUC can be lower than 9 seconds from the start of a rapid decompression to the loss of functional capability.

This paper provides a review of eleven incidents of sudden decompression occurring on commercial airliners during flight, spanned on a period of 1950 to 2011. Relevant details on the source of sudden decompression are also provided. Two specific cases of extreme Hypoxia causing aircraft crashes are also investigated in detail.

The full length paper was presented in the 60th Israel Annual Conference on Aerospace Sciences in 2020 [17].

2.4 An Investigation Into Prying Models in Tension Clips (S. Katzeff, Bird Aerosystems)

Models of the prying phenomena can be split into two types; simple analytical and semi-empirical. Simple analytical models are based on assumptions that, at best, allow for rough sizing, and at worst, are not conservative, and do not address important phenomena. Semi-empirical models attempt to holistically address the various phenomena arising from prying, but are pragmatically focused on matching tested data and arriving at simple design formulae rather than accurately modelling the physical phenomena.

A comparison of these two types of modelling philosophies is presented in this paper, addressing both their advantages and disadvantages. Since most tested data is from the civil engineering-side of the structural fraternity, they apply to end-plate connections with relatively 'thick' bases (>10 mm). The aerospace industry uses 'thin' (<3 mm) bolted tension 'T-clips' extensively to transfer 'light' loads. Accurately predicting the load in the fastener, as well as the bending and shear distribution throughout the clip, is therefore important; especially for fatigue considerations.

To achieve this objective, a method is proposed that assumes the clip to rest on an infinitely stiff, tensionless Winkler foundation. The corner radius is modelled using Castigliano's 2nd theorem to accurately predict the shear and moment distribution throughout the clip. The fastener is modelled as both an axial and torsional spring, allowing for extension and rotation of the fastener, and to establish the point of first contact of the clip with the foundation. Fastener preload is also included in the model. Finally, the maximum applied force at which the clip initiates plastic hinges is also predicted. Predicted results for 'thin' clips match those of 1D Nastran beam models (CBARs) on CGAP elements, as well as a 3D Marc non-linear contact

model (as shown in Figure 8), closer than any other model found in the literature (Figure 9 and Figure 10).

The full length paper was presented in the 60th Israel Annual Conference on Aerospace Sciences in 2020 [18].

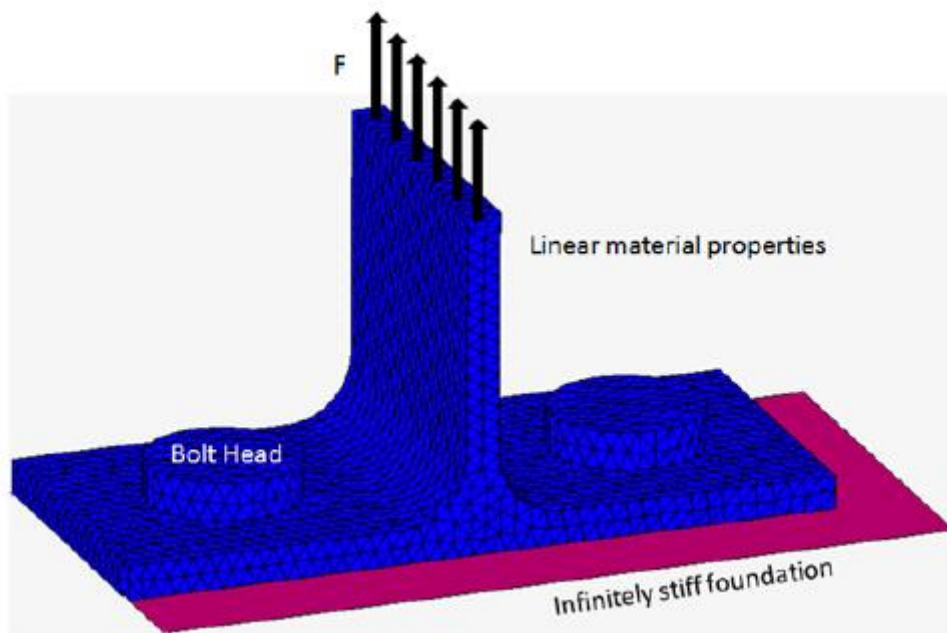


Figure 8: Finite element model used for validation of the analytical approach

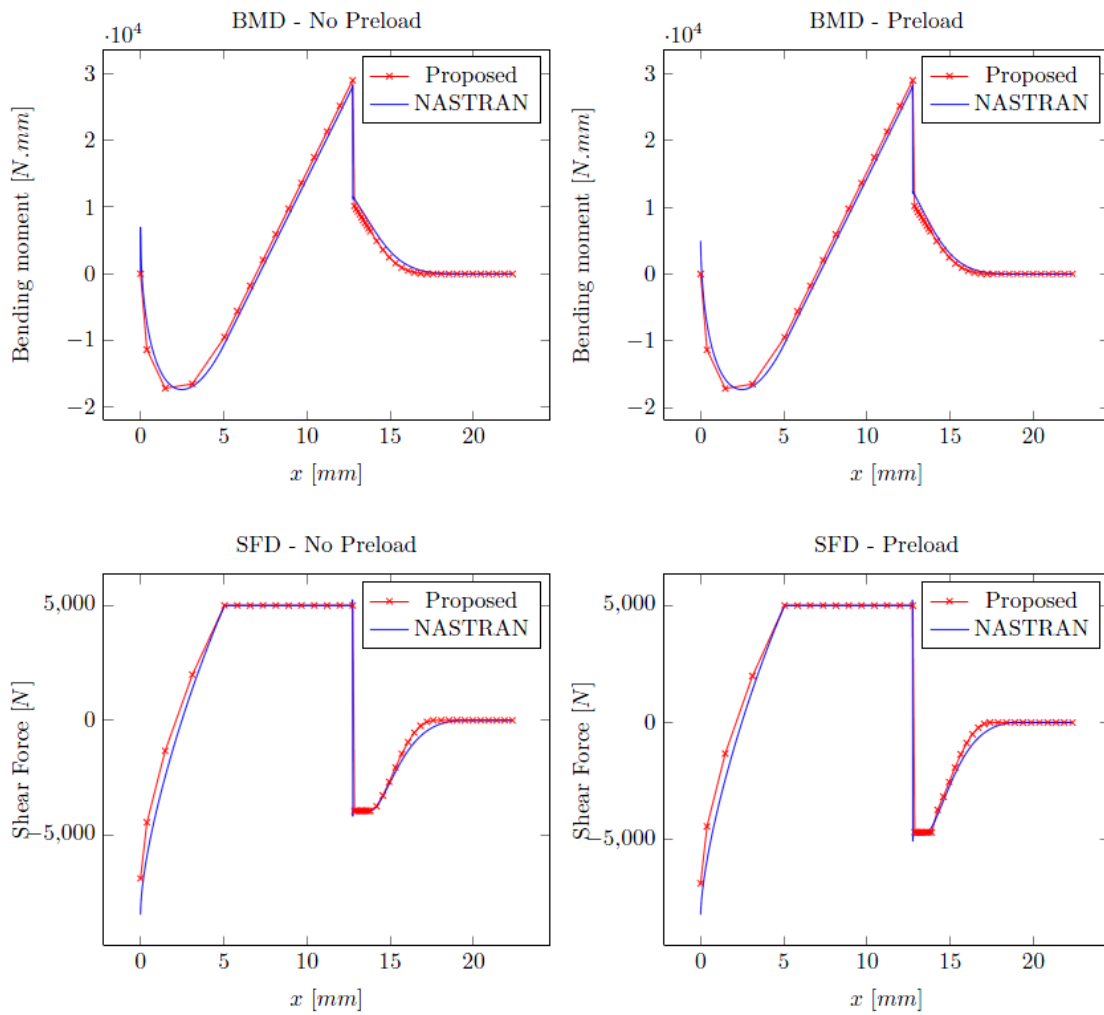


Figure 9: Comparison of results between the proposed approach and a 1-D nonlinear Nastran model

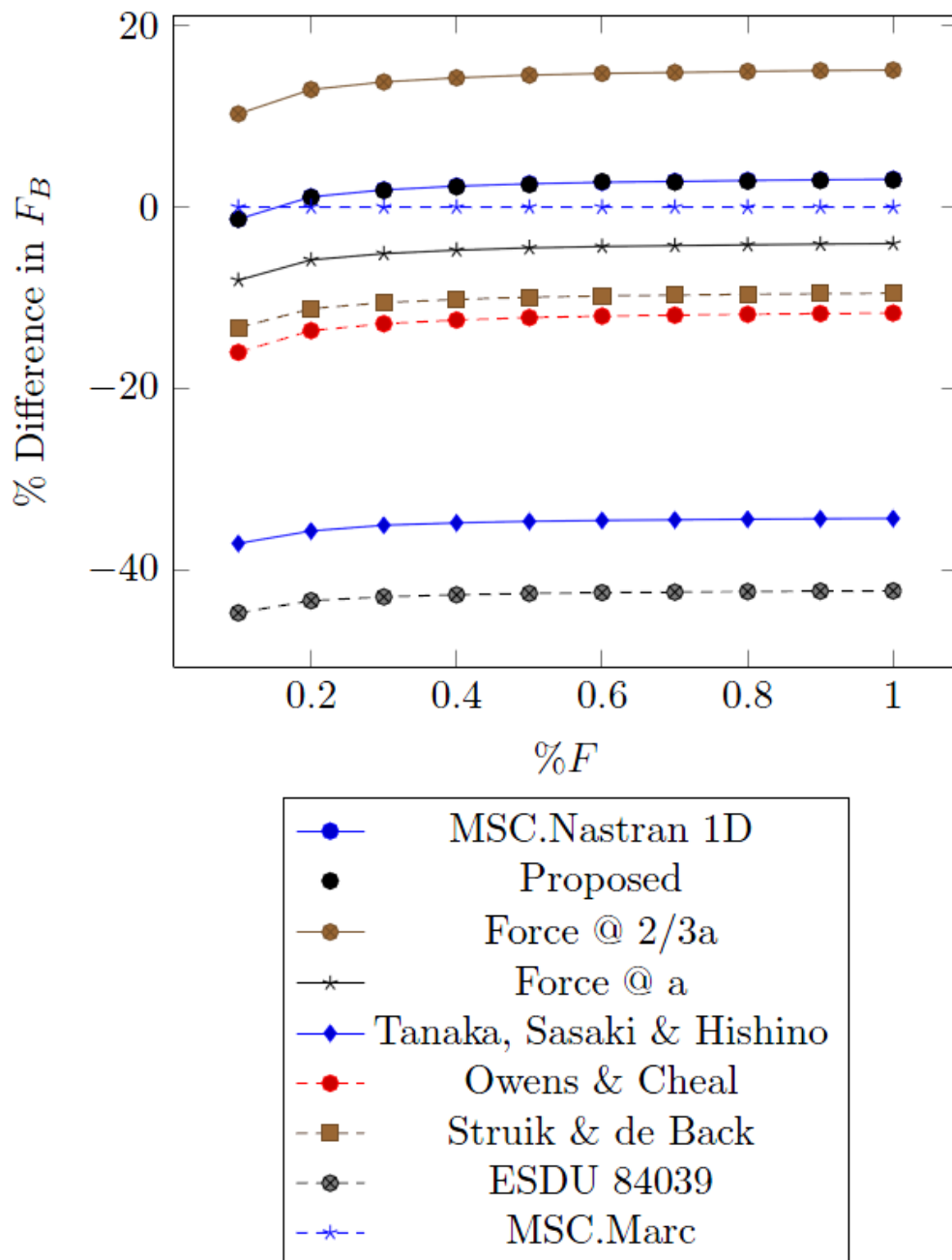


Figure 10: Percentage difference in bolt force compared to MSC.Marc model results; no preload. Similar trend is observed with preload accounted for

2.5 Conversion of 737-800 Passenger to Freighter Aircraft (Y. Freed, IAI)

Israel Aerospace Industries has developed and certified in the past two decades converted freighter for a series of Boeing models, such as 747-200/400, 767-200/300 and 737-300/400/700. Its newest converted freighter, for Boeing 737-800 aircraft, was certified as a supplemental type certificate to the CAAI, FAA and EASA in mid 2020. The conversion includes the installation of a cargo door on the fuselage, additional structural modification to support full load capacity, and implementation of smoke and fire detection in the cargo bay. A solid 9g barrier/smoke partition is installed at aircraft forward fuselage, separating the class E compartment from the occupied area and creating a supernumeraries compartment in the area between the flight deck and the 9g barrier. Interiors, ECS, smoke detection, oxygen, lighting and other systems are modified to accommodate the freighter configuration. The converted B737-800BDSF presents a main deck cargo volume of 4,999 ft³., with lower decks bulk volume of 1,543 ft³, enabling it to carry up to 53,000 lb. An overview of the modifications in the 737-800BDSF aircraft is shown in Figure 11.



Figure 11. Modification at the 737-800BDSF aircraft

The modifications at the aircraft structure include:

- Installation of a Main Deck door surround structure
- Modification of left wing illumination light
- Installation of a Main Deck Cargo Door (MDCD)
- Installation of 9g Rigid Barrier
- Sliding door
- Incorporation of floor beam inspection access

- Installation of three new seat tracks
- Floor beams reinforcements
- Frames reinforcements
- Modification of floor panels
- Installation of Cargo Loading System
- Entry Door deactivation
- Installation of window plugs

Full structural substantiation was conducted to the airframe installations and modifications, as well as full aircraft assessment. The fatigue and damage tolerance substantiation program includes modified inspections to Boeing fatigue critical baseline structure inspections, as well as supplemental inspections to the fatigue critical alteration structure as well as the interface elements between IAI and Boeing structures. A 737-800BDSF in its conversion line is shown in Figure 12.

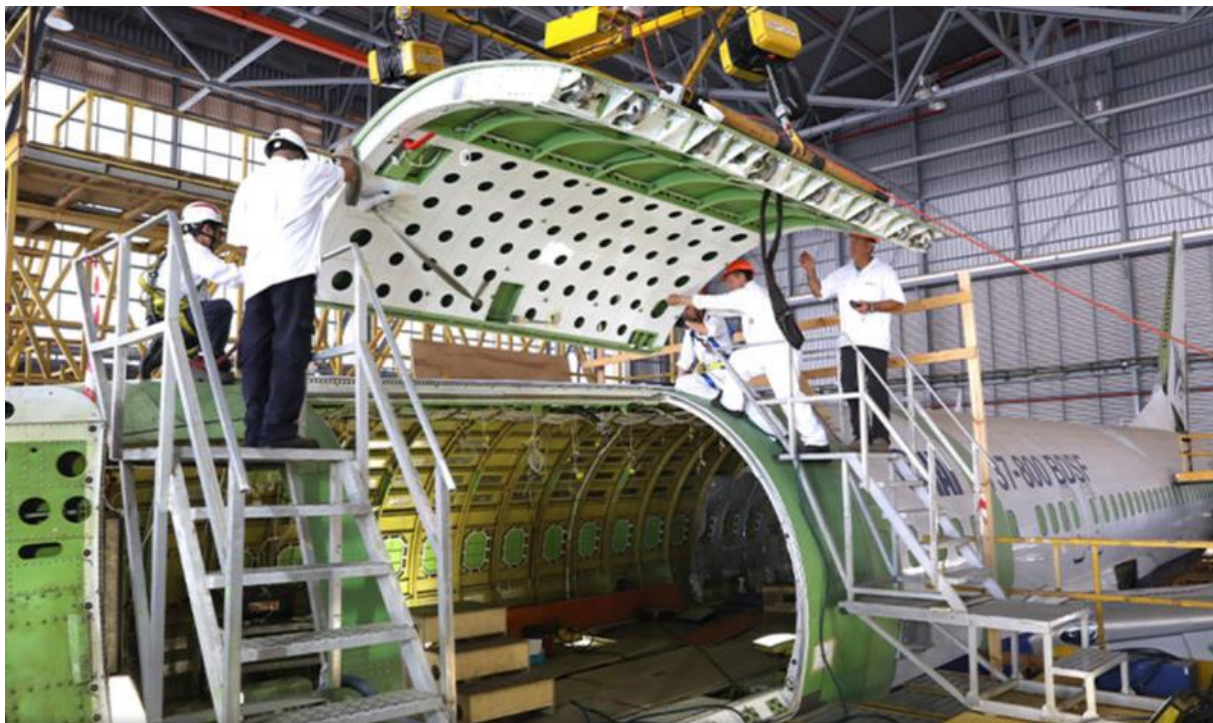


Figure 12. Converted 737-800BDSF aircraft at the conversion line

2.6 Conversion of 777-300ER Passenger to Freighter Aircraft (Y. Freed, IAI)

Israel Aerospace Industries (IAI) entered an agreement in late 2019 with GE Capital Aviation Services (GECAS) on the conversion of passengers' aircraft into cargo configuration. Under the "Big Twin" deal, IAI will convert wide-body, 2-engine Boeing 777-300ER airplanes. The first aircraft is due for delivery to GECAS in 2022. IAI has committed to providing GECAS with 15 converted planes, with an option for 15 additional conversions in the future. This agreement is a formal announcement for IAI to enter the Triple Seven cargo conversions.

The -300ERSF has 47 standard 96 x 125in [2.4 x 3.2m] pallet positions in total. So, overall it has 10 more positions than a 777-200LRF factory freighter or 5,800cb ft [164cb m] more volume. A brochure of the 777-300ERSF is shown in Figure 13.

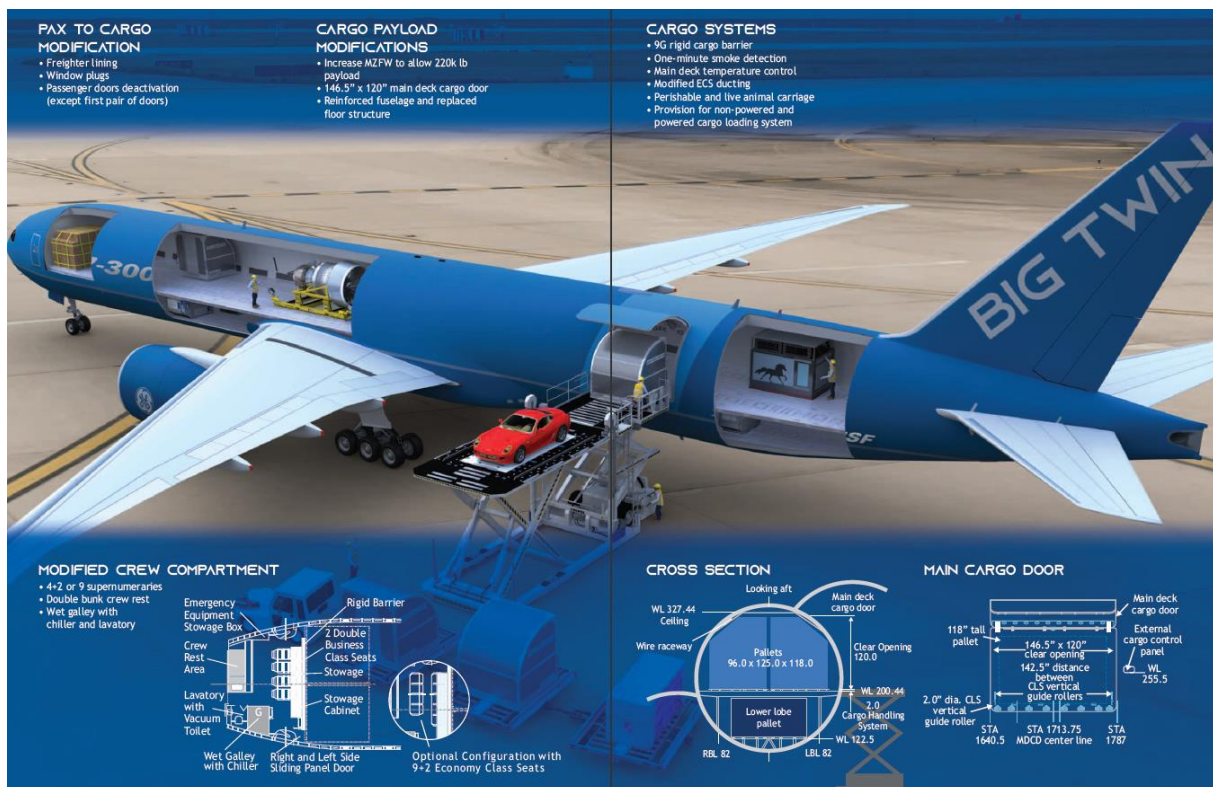


Figure 13. A Brochure of the Converted 777-300ERSF

The progress of the 777-300ERSF conversion development will be reported in future national reviews.



2.7 Research activities in Ben Gurion University – Mordechai Perl Group (M. Perl, BGU)

The research of Prof. Mordechai Perl from Ben Gurion University (BGU) and his co-workers focuses on different aspects of fracture mechanics related to pressure vessels in general, and to the process of autofrettage specifically.

The Stress Intensity Factors (SIFs) of cracked modern tank gun barrel is investigated in Refs. [20, 21]. The combined stress intensity factor K_{IN} consists of two components: K_{IP} —the SIF caused by internal pressure; K_{IA} —the positive SIF due to the tensile residual stresses induced by autofrettage. Ref. [20] investigates the stress intensities for elliptical cracks (with $a/c = 0.2 - 1.0$) and different levels of swage, hydraulic and Hill's autofrettage. Hundreds of different 3-D cases are analyzed by means of finite element models. In Ref. [21], these stress intensities are used for evaluations of the barrel fatigue life due to external cracking. An example of stress intensity factors distributions of an external radial semi-circular of depth $a/t = 0.005$ subjected to three different levels of Hill's, swage and Hydraulic autofrettage is shown in Figure 14.

Rotational autofrettage was investigated in Refs. [22, 23]. Rotational autofrettage is based on inducing plastic deformation in the cylinder at the inner side and at its neighborhood by rotating the cylinder about its own axis at a certain angular velocity and subsequently bringing down it to zero angular velocity. In Ref. [22], the rotational autofrettage for thick-walled cylinders was analyzed theoretically based on the generalized plane strain assumption. The closed form analytical solutions of the elasto-plastic stresses and strains and the residual stresses after unloading during the rotational autofrettage of a thick-walled cylinder were obtained. In Ref. [23], the numerical evaluation of the theoretical model was presented in order to assess its feasibility.

Finally, the interaction between an edge and an embedded parallel cracks is investigated to correlate criteria and standards from various resources in order to recommend the usage of those standards for the purpose of "Fitness-for-Service". In Ref. [24], depending on the crack ratio a_1/a_2 , what may be deemed conservative by one standard, leading to aligned cracks for a given separation distance, H/a_2 and S/a_2 , may be deemed non-conservative, or non-aligned, by another standard. Examples are given in this study demonstrating this phenomenon.

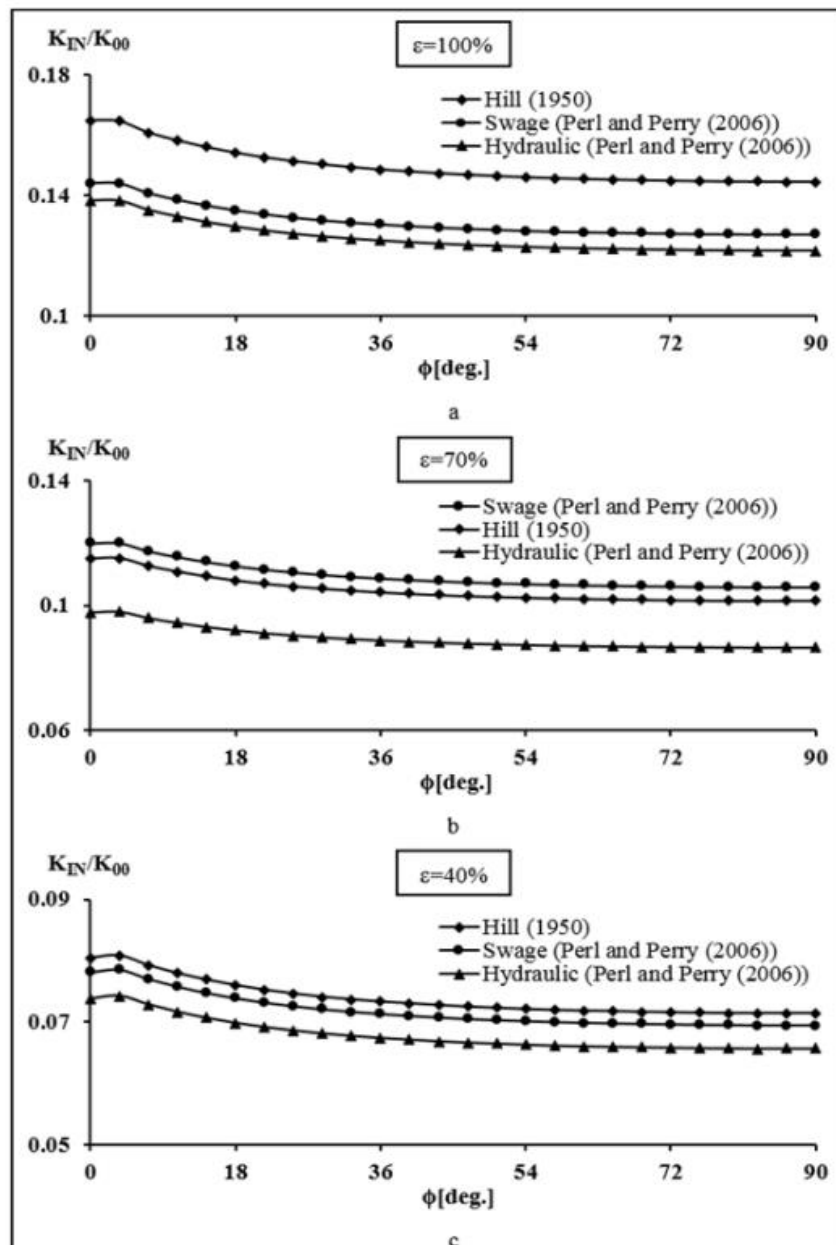


Figure 14. Stress intensity factors distributions of an external radial semi-circular of depth $a/t = 0.005$ subjected to three different levels of Hill's, swage and Hydraulic autofrettage

3. STRUCTURAL INTEGRITY OF COMPOSITE MATERIALS

3.1 Mixed mode failure predictions of adhesively bonded joints based on EA 9294 paste adhesive (Y. Freed and A. Levi Sasson, IAI)

Composite materials are extremely attractive for the aviation industry due to their ability to introduce high stiffness and strength while maintaining low weight. Bonded composite structures (even for large critical structures such as pressure hull and wing box structure) have the potential to be very effective from almost every perspective. They feature a low weight design and demonstrate a dramatic reduction in assembly effort (parts and fasteners count) and related costs. Lockheed Martin demonstrated the possibilities in the mid 1990's during the development of the Advanced Composite Cargo Aircraft, with a 90% parts count reduction in its bonded composite fuselage and vertical tail, and potentially 25% reduction in development costs.

However, even for high quality design, bonded joints still require strict processing control to ensure sufficient quality for the specific materials and processes used for a given structure. Common issues such as improper surface preparation, bond-line contamination, high humidity and insufficient control of cure temperature can cause undetectable low bond-line strengths. As of yet, there is no reliable Non Destructive Inspection (NDI) technique available to adequately ensure that a bonded assembly has retained its full strength. Therefore, the current certification standards require that:

"...the maximum disbonds of each bonded joint consistent with the capability to withstand the loads... must be determined by analysis, tests, or both. Disbonds of each bonded joint greater than this must be prevented by design feature..."

The above mentioned regulatory requirement emphasizes the challenges in insertion of bonded composite joints design to certified aviation products. Comprehensive research should be conducted to provide means for determination of maximum disbonding size, arresting features design and prediction tools for disbond growth and the corresponding residual strength of the joint. In addition, the industry seeks for significant improvements in inspection capabilities, both during assembly and in-service (i.e., condition-based health management), as well as rigorous methodology for determination of the maximum allowed disbond in critical structures to comply with the certification regulations.

This study proposes a failure criterion for the EA 9394 paste adhesive which is commonly used for assembly of large components in the aviation industry. The proposed failure criterion includes the effect of mode mixity as well as the bond line thickness. Comprehensive test campaign was conducted based on Mixed Mode Bending (MMB) specimens for seven different mode mixities and three different bond line thicknesses. The test results were used to obtain failure properties and a von-Mises like failure criterion:

$$\left(\frac{\sigma}{\sigma_{ult.}}\right)^n + \left(\frac{\tau}{\tau_{ult.}}\right)^m = 1$$

Where σ and τ are the tensile and the shear stress obtained by FEM at the disbond tip, σ_{ult} and τ_{ult} are the strength for pure tensile and pure shear conditions, and n and m are constants that were calibrated from the test results.

The MMB test data includes the load to failure versus the test rig displacement. To obtain relevant data for failure predictions of adhesively bonded joints (i.e., σ and τ), finite element model was constructed via StressCheck software. An example of typical finite element model is shown in Figure 15. Since the FEM is linear elastic, the stress concentration at the disbond tip produces very high stresses, which should be limited by the adhesive yield strength. The failure parameters σ and τ were obtained from the FEM along an arc starting from the disbond tip at 45° , identifying the onset of yielding of either the tensile or the shear stresses, whichever occurs first. This initial yield point was taken as the σ and τ combination for the failure criterion. This process was repeated for all mode mixities and bond-line thicknesses.

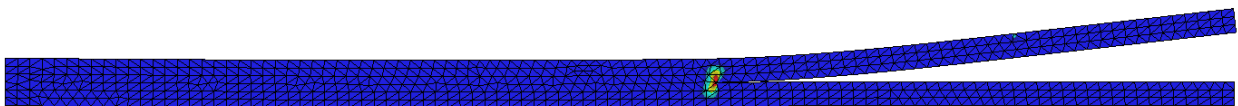


Figure 15: An example of FEM simulation of MMB test

Once the failure parameters for each mode mixity and bond line thickness are in hand, curve fitting using the least squares method was executed. Four mode mixities out of the nine tested (including the pure shear and pure tensile) were used for the curve fitting: $G_{II}/G = 0.5, 0.9$ and pure shear and tension. The remainder of the mode mixities were used for validation of the failure curves, as shown in Figure 16. Very good agreement between the failure envelope and the test results is observed.

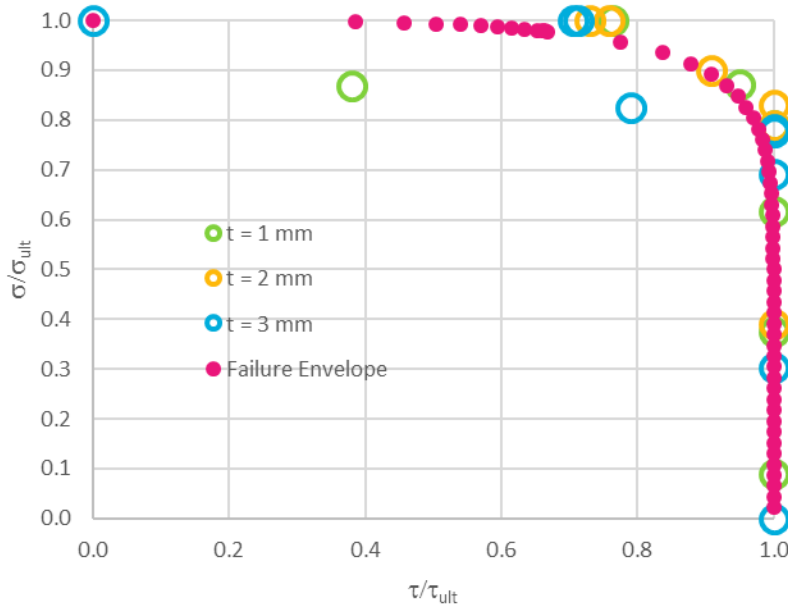


Figure 16: Failure envelope for 9394 adhesive in different thicknesses ($m = 2.4$, $n = 13.4$)

As can be seen from Figure 16, all adhesive thicknesses can be correlated to a single failure criterion. This is due to the fact that the MMB specimen induces almost no secondary bending at the bond line (note the deformed shape of the MMB specimen in Figure 15), as opposed to the classical lap shear specimen. Therefore, increased bond line thickness does not induce significant peeling stresses at the disbond tip. Such behavior is more realistic to typical structural bonding such as wing spar to skins, or fuselage frames to skin, in which secondary bending at the bond line is negligible. For structural bonding representing skins longitudinal splices, in which the secondary bending is significant, other failure criteria are recommended to be used.

A full length paper describing this study was submitted for publications [19].

3.2 The cohesive parametric high-fidelity-generalized-method-of-cells micromechanical model (R. Jaj-Ali, TAU)

The High Fidelity Generalized Method of Cells is a micromechanical approach to obtain strength and stiffness characteristics of multiphase composite materials [25]. Based on the HFGMC approach, the Parametric High Fidelity Generalized Method of Cells (PHFGMC) was derived to include a local cohesive formulation for simulating discontinuities in composite materials.

Ref. 26 presents a comprehensive study comparing the PHFGMC approach with FEM predictions. An example of the accuracy of the PHFGMC method for a case study of a double cantilever beam made of composite materials is shown in Figure 17.

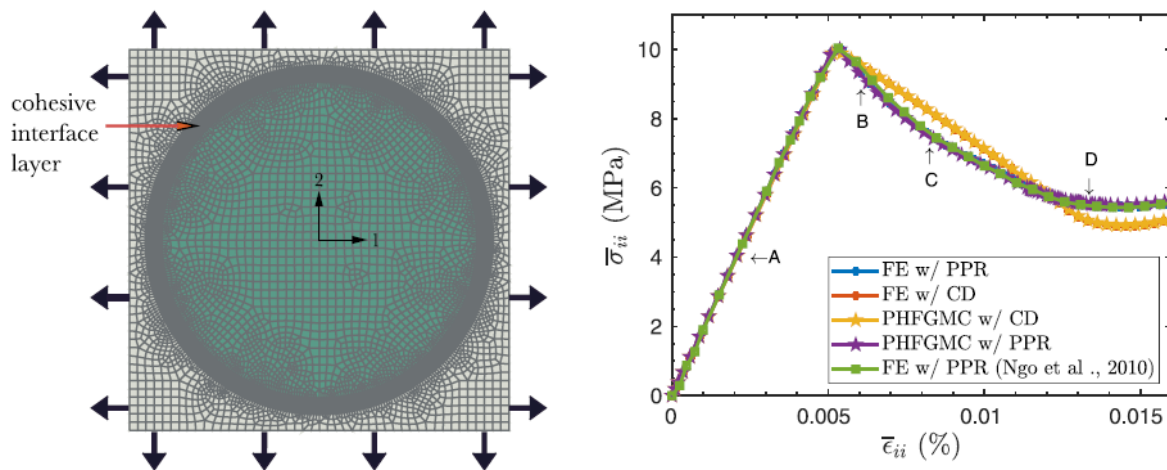


Figure 17: Comparison between PHFGMC and FEM with different cohesive zone traction-separation laws (right) and an overview of a Repeated Unit Cell (RUC) used for the PHFGMC predictions (left)

The full length paper [26] provides a comprehensive overview of the mathematical background for the PHFGMC approach, as well as detail discussions on the failure predictions of the benchmark problem examined.

3.3 OPTICOMS - Optimized Composite Structure for Small Aircraft (A. Sadway, IAI)

Playing an important role within IAI's strategic R&D activities, OPTICOMS is one of several projects within the EU's comprehensive R&D program; Clean Sky 2, in which IAI is not only a participant, but a project leader.

As part of the Airframe module, OPTICOMS is centred around the improvement of aerostructures, namely a wing in the FAR23 class. More specifically, the technical goals of OPTICOMS is to develop an expansive, innovative methodology for low cost, automated composite material aerostructure design, manufacture and substantiation for low volume production.

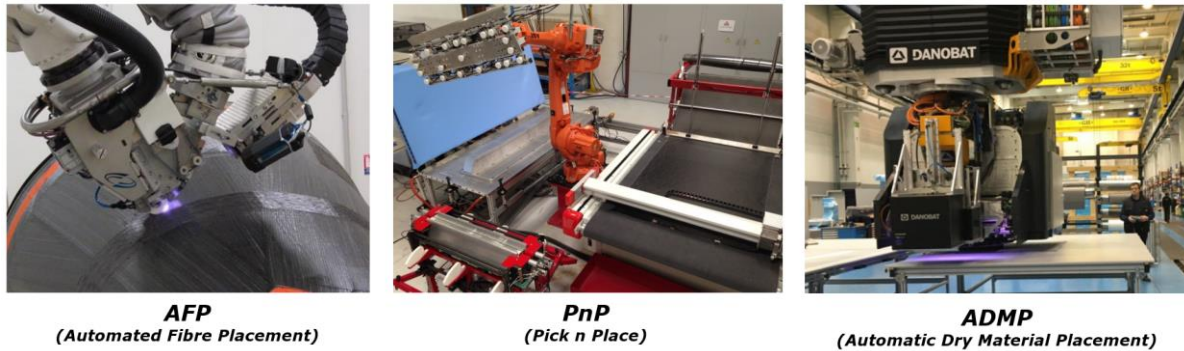


Figure 18: Automated composite manufacturing technologies being assessed in OPTICOMS

Ambitious targets include reductions in production, design & certification and life-cycle costs, along with reduced structure weight. As a means of achieving these targets, key strategic technical guidelines have been defined that include:

- Automated composite manufacture
- DTC (Design to Cost) for low volume production
- Integral structure
- OoA (Out of Autoclave) processes & materials
- Structural bonding

Using the metallic wing of Piaggio Aerospace's P180 Avanti as the baseline, the OPTICOMS consortium (which eventually included over 15 independent European companies) was tasked with producing and substantiating a full-scale, 7m half-wing composite demonstrator. This entire process included the definition, conceptualisation, design, manufacturing (including building block pyramid coupons to elements), finally culminating in a static ground test (as illustrated in Figure 20).

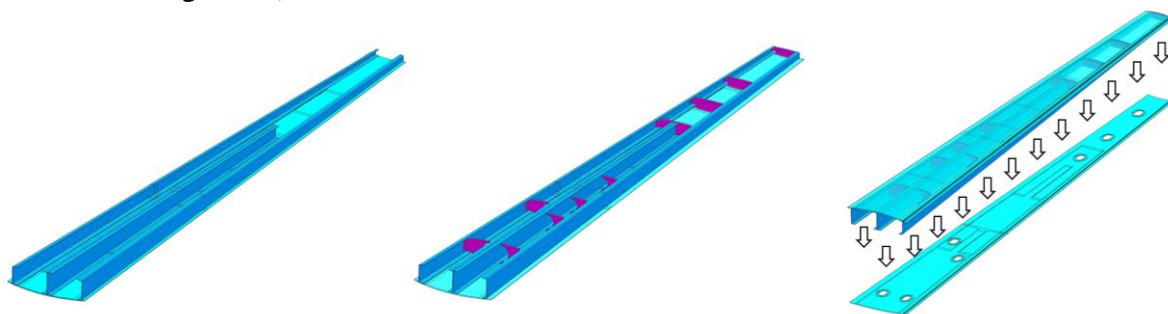


Figure 19: Major manufacturing stages (i) Co-cured skin and spars, (ii) Ribs installation, (iii) Lower skin bonding

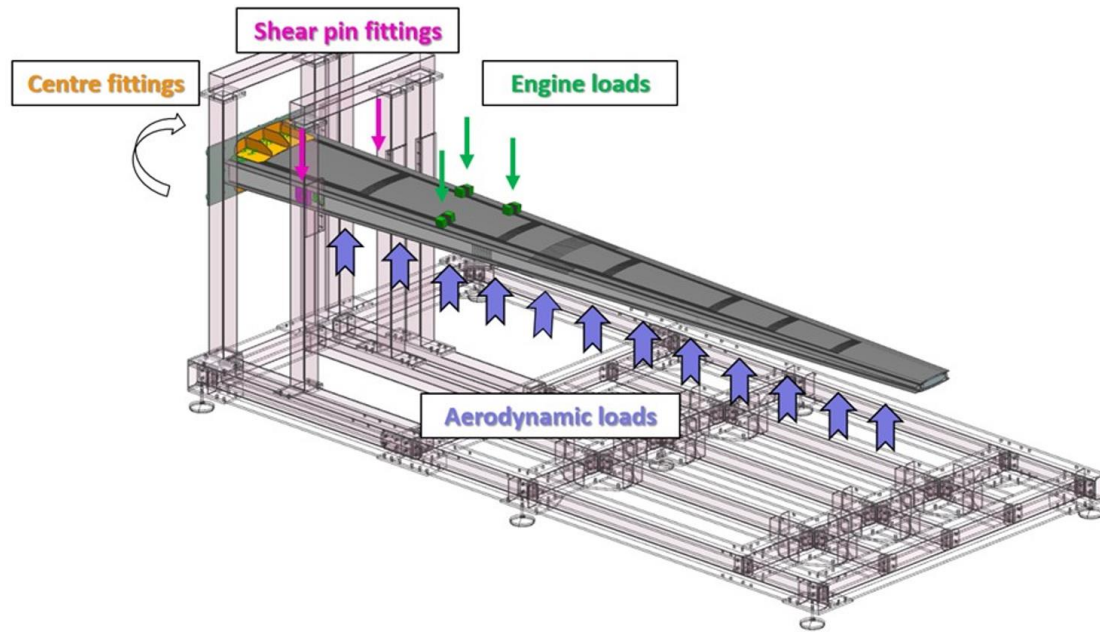


Figure 20: Final static ground test scheme

The project includes supporting activities such as characterization of bond-line strength and failure predictions (as described in Section 3.1), and structural health monitoring of bond-line using optical fibre based sensing technology, all towards future certification of bonded composites.

4. STRUCTURAL HEALTH MONITORING

4.1 A new method for damage identification based on the moving asymptotes approach (F. Kadmany, D. Givoli, O. Rabinovitch, Technion)

This study proposes a new non-destructive method for damage identification that is based upon the moving asymptotes approach. The main idea is based on the fact that a damage induced in a structure can be identified by identification of the stiffness degradation. This degradation is identified by means of an inverse wave analysis.

The identification of stiffness degradation is conducted via a computational model that is based on time dependent measurements of wave propagation. Impact load is applied to the structure, and the waves propagate along it until the damaged zone is reached, and then back to the sensors. Usage of time dependent measurements allows usage of relatively small number of sensors, reduce noise sensitivity and improves detection capabilities.

A benchmark problem is investigated in this research. The identification problem is solved by means of two approaches. First, it is assumed that the damage intensity is known, while the damage location is unknown. In the second approach, both damage intensity and its location are unknown. For the second approach, assuming 181 measurements in time, the damage location ('30' in Figure 21) is easily detected for different damage intensities.

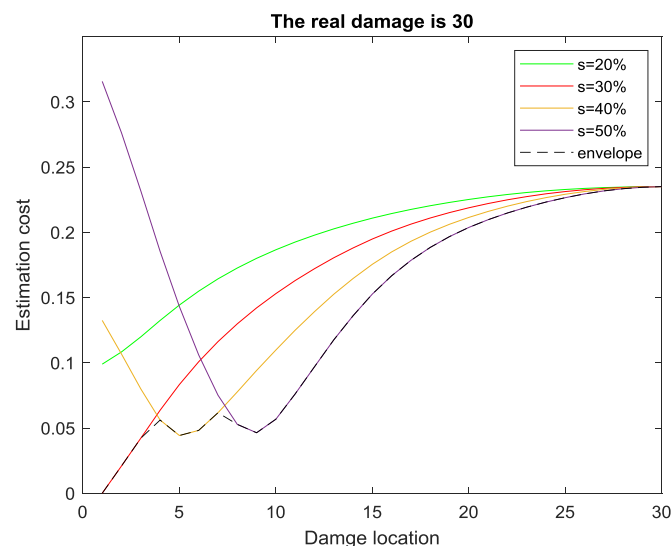


Figure 21: Identification of damage location and size

4.2 Progress at BGU PHM Laboratory (J. Bortman, BGU)

The Ben Gurion University (BGU) Predictive Health Monitoring (PHM) laboratory research methodology for diagnostics and prognostics is physics-based. Each study process is based on physical models (kinematic and dynamic) and experiments with seeded faults. The methodology is based on understanding the physics of the machine components and their expression in the vibration signal in the presence of a fault. Prognostics techniques based solely on empirical data from experiments do not allow generalization of the results. Hence, change in the operating conditions of the monitored system can drastically change the vibration signature and make it difficult to estimate the component state. On the other hand, prognostics methods based solely on models do not guarantee compatibility with real systems. It is important to validate each model against a series of experiments in order to consolidate the physical assumptions and to ensure that the model simulates the reality well enough. Another requirement from the models is that the most important parameters should be considered in the modeling process to increase model credibility and to enable investigation of their influence. Modeling and experiments need to be combined to improve the research process and to reduce the disadvantages of each separate method.

In Ref. 27, the contribution of dynamic models for the development of reliable prognostics and diagnostics algorithms is investigated. The dynamic models enable prediction of changes in dynamic behavior reflecting the fault type and severity using condition indicators and signal processing techniques. A tooth face spall like fault is investigated, as shown in Figure 22.

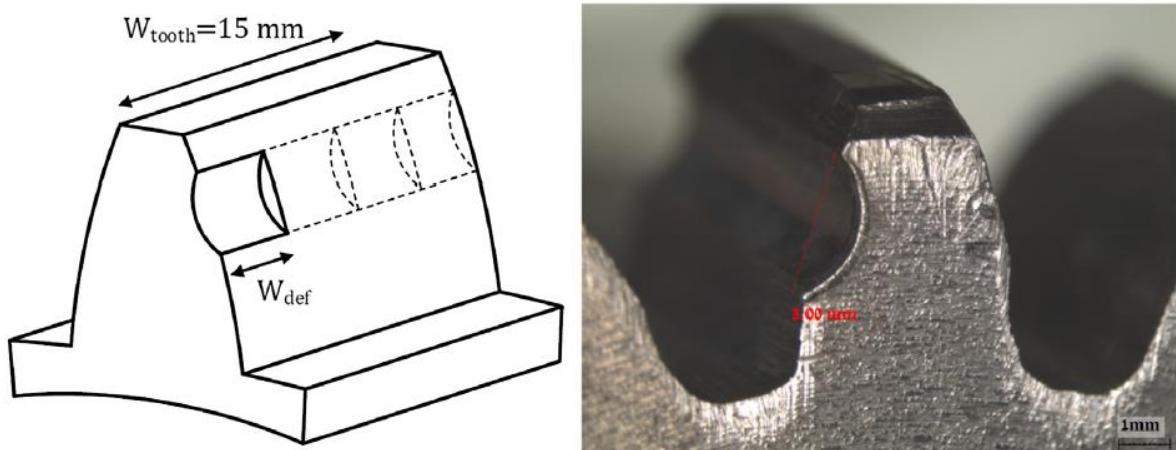


Figure 22: Tooth face spall like fault

The model simulations were compared to the vibrations measured during test. Figure 23 presents the experimental and simulated results. Shaft speed harmonics (related to the support bearings) are marked by black arrows. Most of the peaks in the measured spectrum correspond to one of the test components or one of the supporting bearing tones.

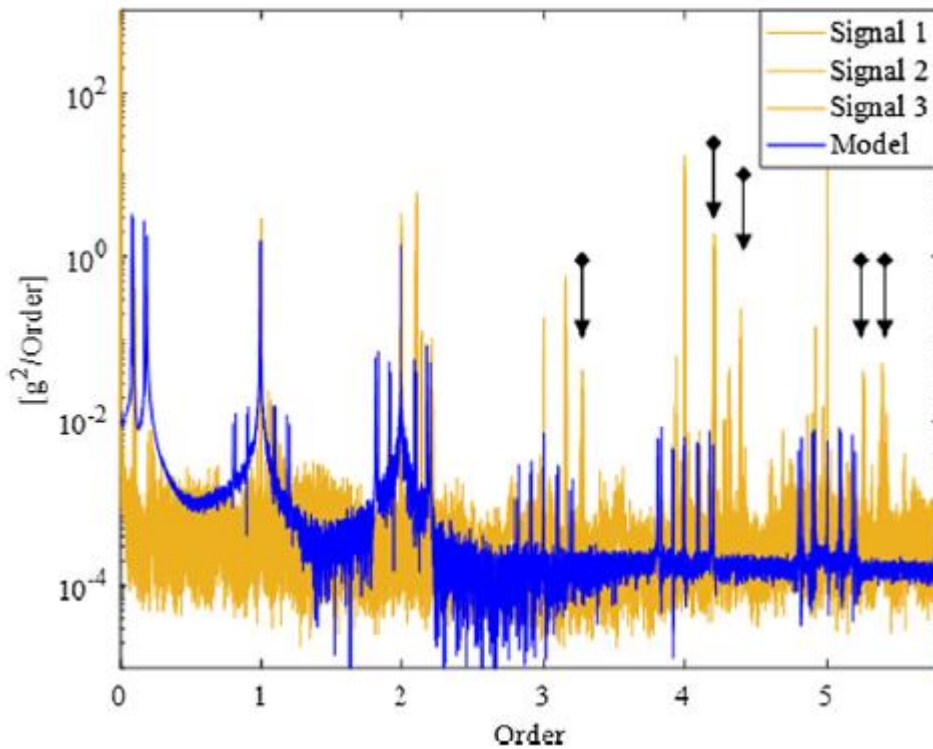


Figure 23: Experimental and test results

In Ref. 28, three different typical failures in gear transmissions were investigated: tooth face fault, broken tooth, and cracks at the tooth root. Example for tooth face fault is shown in Figure 22, while examples for the other faults are given in Figure 24 and Figure 25.

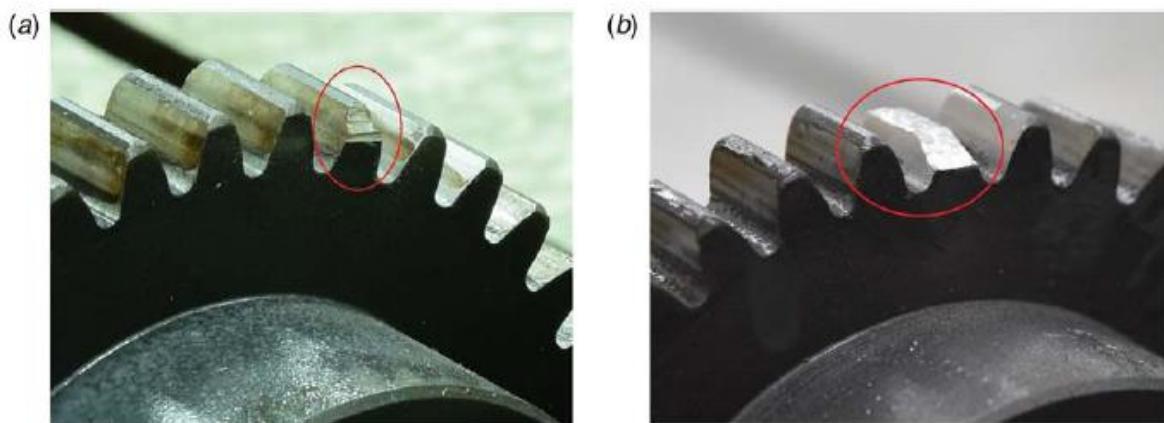


Figure 24: Examples of: (a) chipped tooth and (b) broken tooth

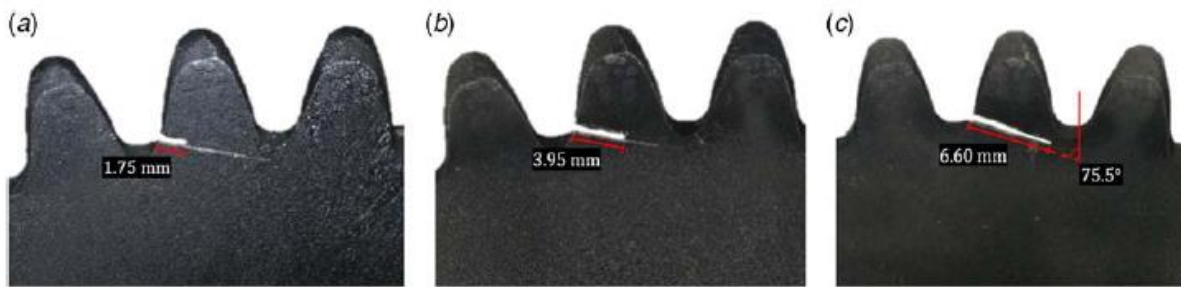


Figure 25: Examples of cracks of different lengths at the tooth root

The faults were thoroughly analyzed to understand the fault manifestation in the vibration signature and to find condition indicators that are sufficiently robust and yet sensitive to the existence and severity of the fault. For each fault, the condition indicators were categorized according to their discrimination power between faulted and healthy states and the ability to rank the fault severity. It was concluded that faults that affect the involute profile throughout the tooth are easily detectable. Faults such as root cracks or chipped tooth, in which mainly the tooth stiffness is affected, are much more challenging to detect.

Ref. 29 describes a new concept for protecting critical mechanical systems against cyber-attacks in which the defense layer is added to the critical rotating machine to prevent hostile entities from damaging it. The machine includes a mechanical component, a Rolling Element Bearing (REB), which acts as a “fuse” mechanism. It is designed so that under cyber-attack the “fuse” REB will be damaged first, ahead of other critical components. Moreover, the defense layer includes Condition Monitoring (CM) tools designed for the “fuse” REB. To the best of the authors knowledge, this is the first study that shows how CM tools can be used as a protective layer against cyber-attack. This study describes the design concepts and focuses on early fault detection and condition monitoring solutions via vibration analysis. Endurance tests were conducted to demonstrate the feasibility of the proposed concept and yield insights into the analysis process of the failure modes that were developed in the “fuse” REB.

In Ref. 30, the “Probability-Based Forest” is proposed. This machine learning algorithm uses a partial physical model with the following steps: First, the behavior of some of the spall sizes is physically modeled and a simulator based on this model generates scenarios for these spall sizes in different conditions. Then, the machine-learning algorithm trains these scenarios to generate a prediction model of spall sizes even for those that have not been modeled by the physical model. Feature extraction is a key factor in the success of this approach, and it is extracted using two traditional approaches: statistical and physical, and an additional new approach: Time Series Feature Extraction based on Scalable Hypothesis tests (TSFRESH). Experimental evaluation with well-known physical model shows that the proposed approach achieves high accuracy, even in cases that have not been modeled by the physical model (see Figure 26 below). Also, it was demonstrated that the TSFRESH feature-extraction approach achieves the highest accuracy.

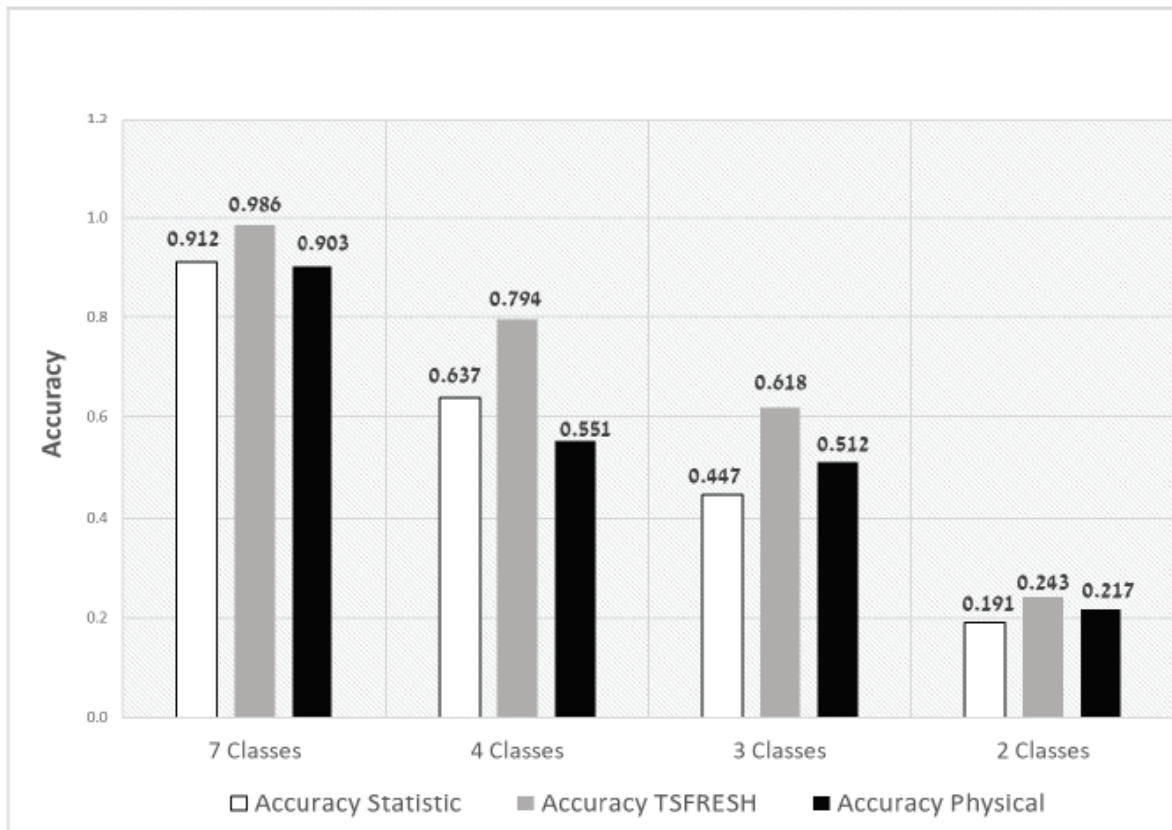


Figure 26: Comparison of the accuracy of the Random Forest classifier for da different number of classes used for training

In Ref. 31, a new method for a reliable modeling of a rolling element spall edge interactions was introduced. The model aims to describe the material response within the spall edge as a result of repeated Rolling Element (RE) impacts. Two complementary RE-spall edge interaction models were developed and integrated, non-linear dynamic and finite element. In order to demonstrate the advantages of the developed model, qualitative damage initiation simulations were conducted. The simulation results were validated and showed a good agreement with the published experimental results. To the best of the authors knowledge, this is the first physics-based attempt to simulate damage evolution within the spall edge.

Ref. 32 provides an example of usage of fiber optics for estimation of damage severity through direct and accurate measurements of damage size and small spalls in the bearing races. Fiber optic sensors are small and can be easily placed in the immediate proximity of the bearing or even embedded inside it, thereby ensuring much enhanced signal-to-noise ratio through the minimizing transmission path effects from remote disturbances. These ball-bearing related diagnostic capabilities of fiber optics sensors are demonstrated via seeded tests, as well as by means of extended monitoring of bearings during fatigue endurance tests. Sensitivity to the sensors location is studied, showing acceptable values at all housing measuring points around the bearing. It was concluded that Fiber-optic sensors appear to have promising diagnostic potential for spall-like faults in both the outer and inner races of ball bearings with a very good discrimination power.

5. MISCELLANEOUS

5.1 Israel's first 3D-printed UAV (I. Kressel, IAI)

The joint program by the Ministry of Defense (MoD) Flight Technologies Department, part of the Directorate for Defense Research and Development, and IAI has seen the production of the SkysPrinter UAV and a successful test flight in December 2019. The electrically powered UAV was made from 26 parts printed using metal, nylon, carbon, and complex materials. These were assembled together with glue and fasteners without the need for specialised tools. SkysPrinter's body is 1.65 m-long, has a wingspan of 1.5 m, and a take-off weight of 7 kg.

The SkysPrinter's modular design allowed for a broad range of adaption to payload requirements. Its main components come apart easily, allowing new parts to be incorporated quickly.

The UAV was printed using a technique known as selective laser sintering (SLS) that allows new designs of the SkysPrinter to be rapidly produced in line with operational feedback from commanders on the ground. SLS technology solidifies polymer materials in precise measurements to produce finalized parts. This way of doing it gives the designers new production capabilities and significant advantages.

In addition, usage of 3D printed techniques leads to significant cost reductions. For example, a 3D-printed UAV similar to the SkysPrinter costs 5,700 USD to produce, while UAVs made with complex material and traditional methods costs about 30,000 USD.

The SkysPrinter had undergone stringent flight tests, including 5G forces, and drop tests. Distributed optical-fibre sensing was used to certify the system for military requirements, with a strain signature distribution in the UAV in resolutions not seen in the past in similar products, down to the level of millimetres.



Figure 27: Skyprinter UAV after take-off

5.2 Additive Manufacturing of Ti-6Al-4V – Develop of Accept/Reject criteria for airframe structure load carry application (C. Matias, IAI)

Additive Manufacturing (AM) of metallic alloys has been deeply investigated in the airframe industry, due to its advantages of short supply chains and supply time, manufacture of complicated geometries in one process for mass production and hence having potential of manufacturing cost reduction.

The AM metallic items implemented today in the airframe industry, are mainly divided into two categories, for the quality control aspects:

- Implementation into secondary structural items that does not participating in carrying flight loads (such as fairings, brackets, etc.). These items generally do not require high levels of quality control as are required for the primary structural items (flight loads carry).
- Implementation into primary structural items (flight loads carrying) – The high level quality control is not applied via universal-standard procedures, but via specified “tailor-made” procedures, of which require great deal of specific development, and usually are not economically feasible for the airframe industry.

In order to further enable implementation of the AM metallic items into the airframe industry, especially for primary structural items, there is a great need for usage of universal-industrial-standard quality control procedures for the quality control assurance (as is done for the traditional technologies). Today such quality control assurance does not exist due to the following reasons:

- The AM presents low level of reproducibility due to its inherent different type of defects, such as: lack of fusion, porosities (air/gas volumes), inclusions, poor surface quality, etc.
- The industry accepted NDT procedures (such as Ultrasonic, Radiography, HFEC/LFEC, Magnetic-Particles, Liquid-Penetrant, etc.) are not effective for such defects detection and monitoring.

Development of industrial-standardized quality control procedure, requires knowledge of:

- The relations between AM different printing parameters and the inherent AM defects
- The relations between the different types of the inherent AM defects to the Fatigue and Damage-Tolerance (FDT) characteristics and data (via tests)
- Acquire knowledge for the critical defect size per the different type of defects (via the FDT aspects) and prove of such defects detection and monitoring (via repeated procedure) towards a procedure for Accept/Reject Criteria to AM Structural Items

This study investigates the above three issues upon Ti-6Al-4V. The study is financed by the Israeli Ministry of Economy and Industry – the Israel Innovation Authority. The study is a team effort by the following three parties:

- Israel Aerospace Industries (IAI) – The program manager
- Israel Institute of Metals (IIM), Technion, Israel Institute of Technology – Developing the Printing and monitoring parameters (via EOS-M290 ALM LBM), preparing the Specimens and conducting the tests (Static, Crack-Initiation and da/dN crack growth tests).
- AFEKA College, The Materials and Processes Center – Defects investigation (via a powerful micro-CT NDI equipment), and Fractographic & Failure Investigation.

Figure 28 presents example from the Printing MPM investigation results and from the Micro-CT inspection results, and the correlation between the two.

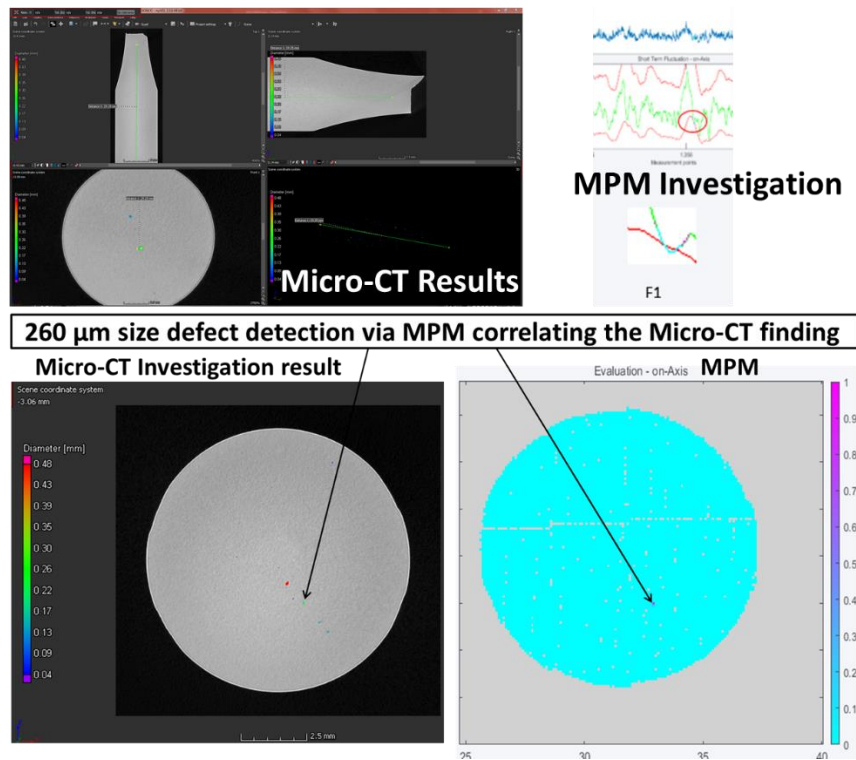


Figure 28: Correlations between printing MPM investigation results and Micro-CT inspections

Figure 29 presents the crack-initiation and da/dN test results for the different 4 printing parameters configuration sets performed in the study. Tray #1 printing parameters are the EOS machine defaults, resulting in Weibull characteristic life of about 5,200,000 cycles. Note that all specimens did not perform HIP procedure (HIP procedure is done for next program stage). Tray #2 introduces a change in printing parameters that improved the fatigue results to Weibull characteristic life of about 9,500,000 cycles (as HIP result). Trays #3 & #4 introduce changes in printing parameters that create lots of defects and their fatigue life is very low (~6,000 & ~1,000 cycles respectively). It is interesting to notice that for all the printing parameter configurations (the “good” & the “bad”), the da/dN test results does not present much differences or variations, and are relatively close to the accepted NASGRO® da/dN data for Ti-6Al-4V alloys (Plate & Forging).

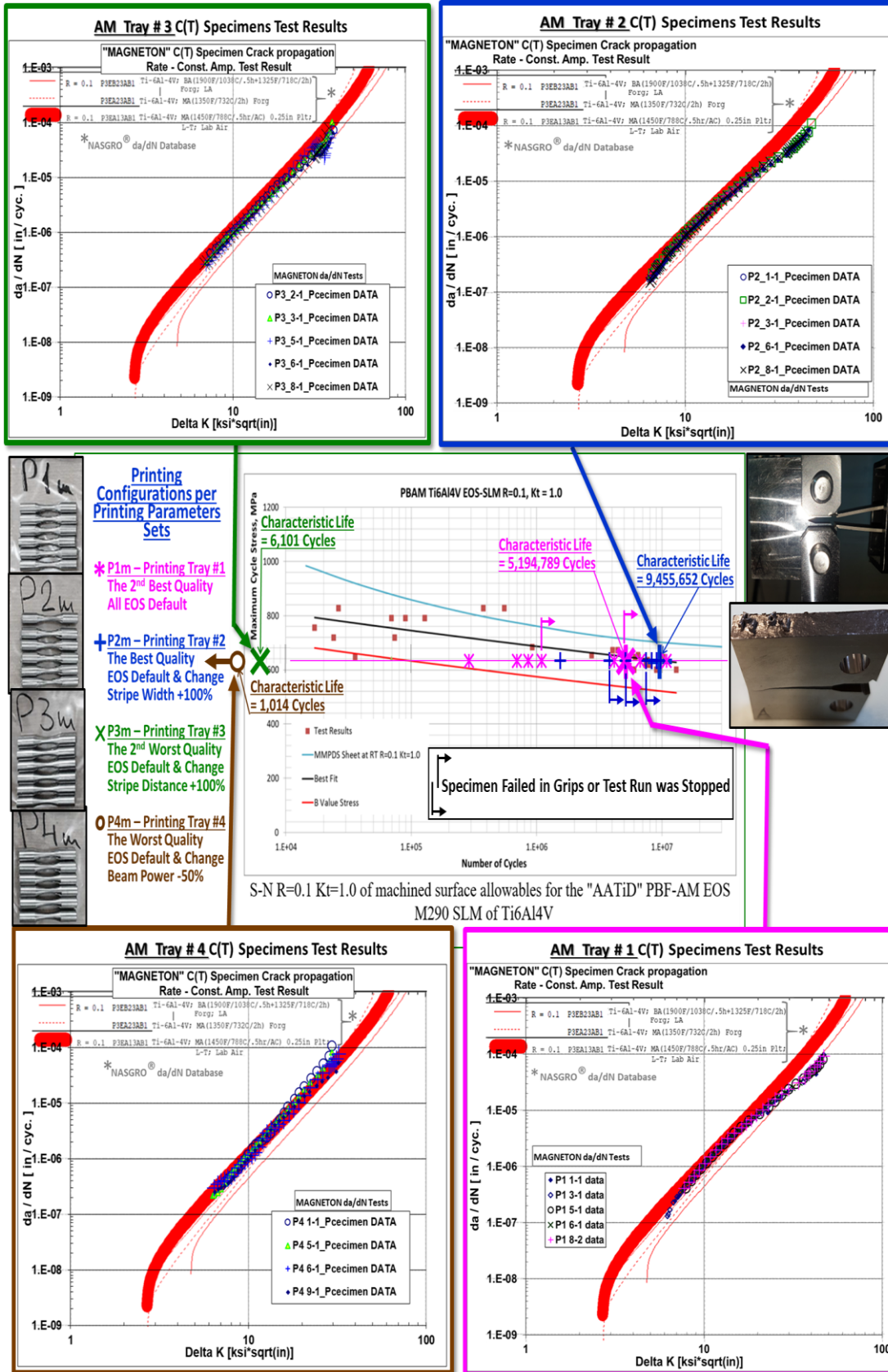


Figure 29: Crack-initiation and da-dN test results for four printing parameters configurations

7 REFERENCES

1. Freed Y., “Review of Aeronautical Fatigue Investigations in Israel, January 2017 – December 2018”, *Minutes of the 36th ICAF Conference*, Krakow, Poland, 2017.
2. Freed Y., Widespread Fatigue Damage Assessment – What can possibly go wrong?, *59th Israel Annual conference on Aerospace Sciences*, 2019, Haifa, Israel.
3. Elmalich D., Brot A., Freed Y., Buimovich Y., and Matias C., A risk analysis based methodology for widespread fatigue damage assessment, *55th Israel Annual conference on Aerospace Sciences*, 2015, Tel Aviv, Israel.
4. Freed Y., Elmalich D., Brot A., Buimovich Y., and Matias C., A risk analysis based methodology for widespread fatigue damage evaluation, *28th ICAF symposium*, 2015, Helsinki, Finland.
5. Airworthiness Directive (AD) 2002-07-08.
6. National Transportation Safety Board report, NTSB/AAB-13/02, dated: 24.9.2013.
7. Hartman A. and Schijve J., The effect of secondary bending on the fatigue strength of 2024-T3, NLR, Amsterdam, Technical Report 69116, 1969.
8. Schijve J., *Fatigue of structures and materials*, Dordrecht, The Netherlands, Springer, 2001.
9. De Rijck J.J.M, Stress analysis of fatigue cracks in mechanically fastened joints. An analytical and experimental investigation. PhD Thesis, Delft University of Technology, 2005.
10. Schijve J., Riveted lap joints with a staggered thickness in the overlap of the joint. Calculations of secondary bending, Faculty of Aerospace Engineering, Delft, 2006 [Doc. B2-06-02].
11. Schijve J. and Campoli G., Fatigue of structures and secondary bending in structural elements, *International Journal of Fatigue*, 2009, DOI: 10.1016/j.ijfatigue.2009.01.009.
12. Skorupa M. et al., Observation and analyses of secondary bending for riveted lap joints, *International Journal of Fatigue* 72, p. 1-10, 2015.
13. Skorupa M. et al., Fatigue strength reduction factors at rivet holes for aircraft fuselage lap joints, *International Journal of Fatigue* 80, p. 417-425, 2015.
14. Freed Y et al., Numerical Investigation of the Effect of Secondary Bending in Hard-point Joints, *59th Israel Annual conference on Aerospace Sciences*, 2019, Haifa, Israel.
15. Freed Y. et al., Analytical and Numerical Investigation of the Effect of Secondary Bending in Hard-point Joints, 30th ICAF symposium, 2019, Krakow, Poland.

16. Freed Y. Investigation of the Effect of Secondary Bending on Multi-Site Damage Scenarios in Hard-point Joints, *60th Israel Annual conference on Aerospace Sciences*, 2020, Tel Aviv, Israel.
17. Brot, A., Loss of Useful Consciousness Aboard an Aircraft due to a Lack of Oxygen, *60th Israel Annual conference on Aerospace Sciences*, 2020, Tel Aviv, Israel.
18. Katzeff, S., An Investigation Into Prying Models in Tension Clips, *60th Israel Annual conference on Aerospace Sciences*, 2020, Tel Aviv, Israel.
19. Levi Sasson A. and Freed Y., Mixed Mode Failure Predictions of Adhesively Bonded Joints Based on EA 9294 Paste Adhesive, Submitted for Publication.
20. Perl, M., and Saley, T., The Detrimental Effect of Swage and Hydraulic Autofrettage on Externally Cracked Modern Gun Barrels, *Defence Technology*, 15 (2019) pp. 146-153.
21. Perl, M., and Saley, T., The Cumulative Detrimental Impact of Pressure and Autofrettage on the Fatigue Life of an Externally Cracked Modern Tank Gun Barrel, *AIMS Materials Science*, 2019, Vol. 6(5), pp. 833-851.
22. Kamal, S. M., Perl, M., and Bharali, D., Generalized Plane Strain Study Rotational Autofrettage of Thick-walled Cylinders, Part I– Theoretical analysis, *Trans. of the ASME, Journal of Pressure Vessel Technology*, 141(5), 051201 (2019), (11 pages).
23. Kamal, S. M., and Perl, M., Generalized Plane Strain Study Rotational Autofrettage of Thick-walled Cylinders, Part II– Numerical Evaluation, *Trans. of the ASME, Journal of Pressure Vessel Technology*, 141(5), 051202 (2019), (7 pages).
24. Ma, Q., Levy, C., and Perl, M., The Interaction between an Edge and an Embedded Parallel Crack in a Structural Component, *Modern Civil and Structural Engineering*, Vol. 4, No.1, (2020).
25. Aboudi, J., The generalized method of cells and high-fidelity generalized method of cells micromechanical models – a review:, *Mechanics of Advanced Materials and Structures* 11 (4-5), p. 329-366, 2004.
26. Meshi, I. et al., The cohesive parametric high-fidelity-generalized-method-of-cells micromechanical model, *International Journal of Solids and Structures* 206, p. 183-197, 2020.
27. Madar, E., Klein, R. and Bortman, J., Contribution of dynamic modeling to prognostics of rotating machinery, *Mechanical Systems and Signal Processing* 123, p. 496-512, 2019
28. Dadon, I. et al., A step toward fault type and severity characterization in spur gears, *Journal of Mechanical Design* 141, 2019.
29. Gazizulin, D. et al., Critical rotating machinery protection by integration of a “fuse” bearing, *International Journal of Critical Infrastructure Protection* 27, 2019
30. Tam, I. et al., Probability-based algorithm for bearing diagnosis with untrained spall sizes, *Sensors* 20, 2020, doi: 10.3390/s20051298.



31. Gazizulin D. et al., A new efficient rolling element – spall edge interaction model, International Journal of Fatigue 131, 2020
32. Alian, H. et al., Bearing fault detection and fault size estimation using fiber optic sensors, Mechanical Systems and Signal Processing 120, p. 329-407, 2019